# In-plane Raman scattering of (001)-Si/Ge superlattices: Theory and experiment

R. Schorer and G. Abstreiter
*Walter Schottky Institut, Technische Universität München, D-85748 Garching, Germany*

S. de Gironcoli
*INFM Institute of Condensed Matter Theory (FORUM), Scuola Normale Superiore, Piazza dei Cavalieri 7, I-56100 Pisa, Italy*

E. Molinari
*Dipartimento di Fisica, Università di Modena, Via Campi 213/a, I-41100 Modena, Italy*

H. Kibbel and H. Presting
*Daimler-Benz AG, Research Center Ulm, Wilhelm-Runge-Strasse 11, D-89081 Ulm, Germany*
(Received 13 September 1993)

Using a micro-Raman setup, in-plane Raman scattering was performed on short-period (001)-Si/Ge superlattices, and the complete phonon spectrum (longitudinal and transverse, optical and acoustic modes) could be studied. In the relevant wave-vector range, the in-plane dispersion was found to affect the frequencies of folded-acoustic modes, while being negligible for confined optical modes. The comparison with theoretical spectra, calculated by means of first-principles interatomic force constants, shows that the observed deviations of "unfolded" confined optical modes from the bulk dispersions can be attributed to interface roughness and is well described by a simple alloy layer model (2–3 intermixed SiGe atomic layers at interfaces).

## I. INTRODUCTION

In recent years there has been considerable interest in Si/Ge superlattices (SL's) since they provide a possibility to overcome the restrictions in the optical and electronic properties of bulk Si as compared to III-V semiconductors.[1,2] Short-period Si/Ge SL's have proven to be promising candidates for quasidirect band-gap luminescence.[3] Raman spectroscopy is a useful tool for characterizing short-period SL's, since their vibrational properties depend strongly on their microscopic structure.[4]

Conventionally, Raman scattering is performed in backscattering from the growth direction (usually the [001] direction). In this case, from the (001) surface only longitudinal modes are observable off resonance. In order to establish a full picture of the vibrational modes of SL's, their symmetry, and their coupling to light, it is necessary to perform Raman scattering along each primitive axis of the SL crystal. Such a full analysis was recently presented for the optical-phonon modes of (001)-GaAs/AlAs SL's,[5,6] where in-plane studies were shown to be possible by reducing the probe laster spot to a sub-$\mu$m focus (micro-Raman scattering). Using this approach, we are now able to study the quantized longitudinal-optical (LO) and transverse-optical (TO) modes, as well as the folded longitudinal-acoustic (LA) and transverse-acoustic (TA) ones in our Si/Ge structures.

A similar improvement has recently taken place on the theoretical side. Earlier *ab initio* treatments[7] of the phonon spectra were limited to modes with wave vectors along the growth direction, for which one-dimensional approaches could successfully be adopted. Just recently we have been able to extend first-principles studies to three-dimensional SL dispersions by using higher-order interatomic force constants which allow us to account for both strain and interface intermixing.[8,9]

The aim of this paper is to describe the features found in the experimental Raman spectra, and to compare them with theoretical predictions. In particular, we shall focus on the confinement properties of Si-like longitudinal and transverse vibrations, and on the behavior of higher-order acoustic modes. The specific properties of the Si-Ge-like interface mode have been reported elsewhere[9] and will be only briefly summarized here. We will show that experimental spectra deviate significantly from the theoretical spectra expected for abrupt-interface geometries. On the other hand, by taking into account interface intermixing (2–3 monolayers of SiGe alloy at the interfaces) a general agreement between theory and experiments is recovered.

The paper is organized as follows. Section II gives a brief illustration of the sample preparation and the experimental technique, while Sec. III summarizes the essential features of our theoretical approach. Section IV presents our results for the optical frequency range: We first recall the general features of the LO- and TO-phonon spectra of ideal SL's, and discuss the reliability of simple "unfolding" rules for confined SL modes. Systematic experimental results for a series of (001)-$Si_n/Ge_n$ SL's are reported and discussed in terms of these "unfolding" rules. The analysis of the observed deviations is then performed on the basis of a detailed treatment of disorder effects. Section V is devoted to acoustic modes, while Sec. VI contains a general discussion and comparison with GaAs/AlAs SL's, together with our conclusions.

0163-1829/94/49(8)/5406(9)/$06.00  

## II. EXPERIMENTAL TECHNIQUE

The samples were grown by low-temperature molecular-beam epitaxy (MBE) on Si(001) and Ge(001) substrates, using Sb as a surfactant layer. Strain symmetrization was achieved by using a 200-Å partially relaxed $Si_{0.25}Ge_{0.75}$ alloy buffer layer. The total SL thicknesses are between 0.2 and 1.0 $\mu$m. Typical flux rates were $R \cong 0.3$ Å/s for Si and Ge, with substrate temperature $T_s \cong 310$ °C. More details on substrate preparation, growth conditions, and characterization are given in Ref. 11.

In our Raman experiments, a microscopic objective was used for focusing and collecting the light. The power density was kept below $10^5$ W/cm$^2$ in order to preclude sample heating. The measurements were performed at room temperature with the 514.5-nm line of an $Ar^+$ laser, and with a dye laster at 598 nm, using a triple-grating spectrometer in the subtractive mode with a spectral resolution of 2.5 cm$^{-1}$. The excitation energy is near the $E_1+\Delta_1$ gap of Ge (near-resonance condition). The signal was detected with a cooled photodiode multichannel detector. A reduction of the stray light was achieved by tilting the normal of the surface away by about 30° with respect to the incident light. The large refraction index ($n \cong 4$) helps to significantly reduce the deviation from ideal backscattering conditions caused by the relatively large aperture of the lens and the inclination of the sample surface. The scattering configurations we have used are shown in the insets of Fig. 4 below. The labeling of the axes—$x \| [001]$, $y \| [010]$, $z \| [001]$, where $z$ is the growth direction—refers to the cubic conventional unit cell of the bulk materials. Also, a second coordinate system with $x' \| [1-10]$, $y' \| [110]$, $z'=z$ is used.

## III. THEORETICAL APPROACH

As in previous studies of $Al_xGa_{1-x}As$-based heterostructures,[12] we have chosen to use accurate interatomic force constants which are calculated from first principles within density-functional theory in the local-density approximation by means of a linear-response scheme. The ability of such force constants to reproduce the bulk vibrational properties of Si and Ge was demonstrated in Ref. 8 (see also the comparison between theoretical and experimental $\Gamma$-$X$ dispersions in Fig. 1). In order to extend this approach to Si/Ge heterostructures, however, additional difficulties related to strain effects have to be faced. Such effects include homogeneous strain induced by lattice matching to the substrate, as well as local bond-length variations depending on the local atomic configuration in regions of mixed SiGe composition. As shown in Ref. 8, this problem can be solved by using higher-order interatomic force constants, which are also obtained within a first-principles scheme.

To model SL's with disordered layers, an additional periodicity in the $xy$ plane parallel to the interfaces has been assumed; Si and Ge atoms in the alloyed planes are distributed at random in an 18-atom two-dimensional unit cell according to the given concentration, and the calculated properties are averaged over $\approx 10$ different configurations. Phonon spectra (frequencies and displacement profiles) are then obtained by direct diagonalization of the dynamical matrix, and the corresponding Raman strengths are estimated assuming the same bond polarizability in both materials. We consider the latter approximation acceptable because we are mostly interested in comparing Raman intensities of modes having the same origin.

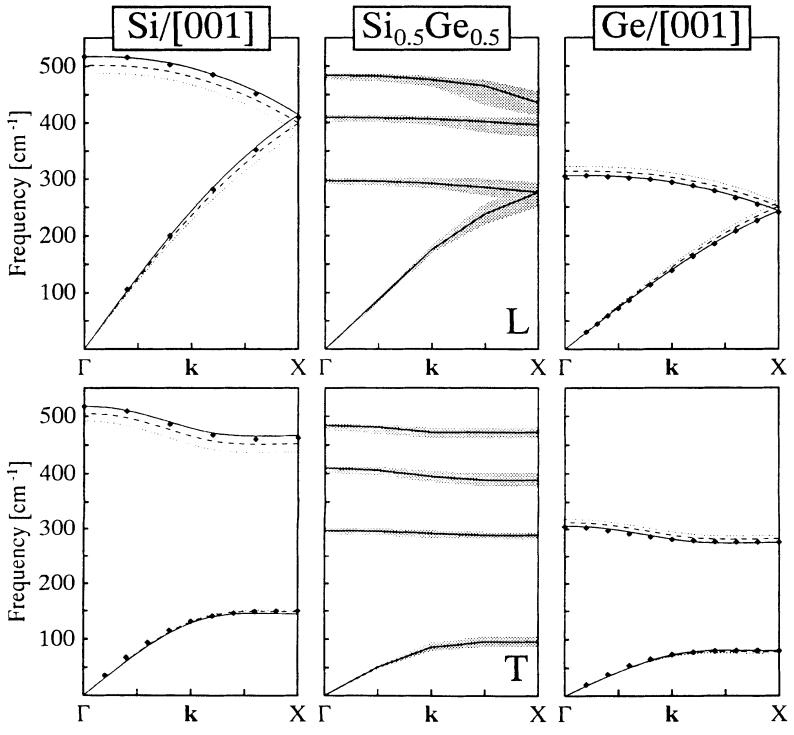


FIG. 1. Calculated bulk dispersions along (001) for Si and Ge and the $Si_{0.5}Ge_{0.5}$ alloy. $L$ and $T$ polarizations are shown in the top and bottom panels, respectively. For Si and Ge, different strain configurations are shown: unstrained (solid lines), and lattice matched to the $Si_{0.5}Ge_{0.5}$ alloy (dashed lines) or to the other semiconductor (dotted lines). The symbols are neutron-scattering data for the unstrained configuration. The shaded lines in the central panel indicate the width of the alloy quasi-dispersion (see Ref. 9).

As a reference for the forthcoming discussion on SL spectra, in Fig. 1 we report the calculated $L$ and $T$ dispersions of bulk Si and Ge along the [001] direction. Besides the curves for the unstrained case (solid lines), which are compared with neutron-scattering data[13] (full symbols), we also show by dashed lines the dispersions obtained for a biaxial strain configuration corresponding to lattice matching to a $Si_{0.5}Ge_{0.5}$ alloy substrate (compressive strain for Ge, and dilational strain for Si); dotted lines correspond to lattice matching of Si to Ge and vice versa. Moreover, in the central panels we show the $L$ and $T$ quasidispersions calculated for the unstrained $Si_{0.5}Ge_{0.5}$ alloy.[14]

## IV. OPTICAL MODES

### A. Theoretical predictions for ideal superlattices: "unfolding" rules, in-plane dispersion

To introduce notations, let us first recall the main features that are known to characterize the optical-phonon spectrum of (001)-Si/Ge SL's with ideally abrupt interfaces. We refer to Fig. 2, where a strain-symmetrized $Si_8/Ge_8$ SL is taken as an example.

For wave vectors along the (001) direction (right-hand panel of Fig. 2) the $L$ and $T$ polarizations are decoupled (solid and dashed lines, respectively). Above $\approx 310$ cm$^{-1}$ (upper edge of the $L$ dispersion of strained Ge, see Fig. 1), $L$ modes are nondispersive, reflecting confinement in the Si layer (Si-like modes). Around and below 310 cm$^{-1}$, $L$ Ge-like resonant modes exist, which have a maximum amplitude in the Ge layer but an oscillatory behavior also in the Si layers (quasiconfined modes).[15] The situation is different for the $T$ polarization. Here the bulk TO branches of Si and Ge do not overlap in frequency, so that SL modes are confined either in the Si or Ge regions.

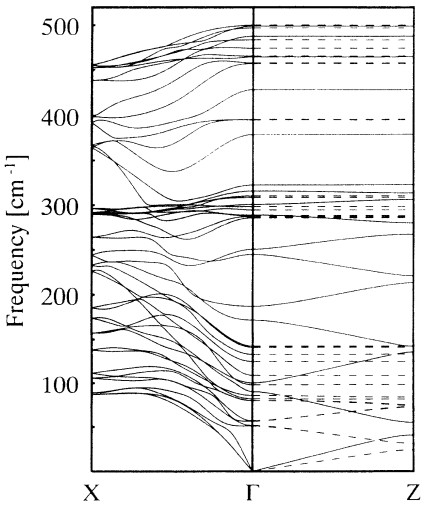


FIG. 2. Calculated dispersion for an ideal $Si_8/Ge_8$ SL along the [001] growth direction (right-hand panel), and along the [100] in-plane direction. For [001] propagation, the $L$ and $T$ polarizations are decoupled, and are indicated by solid and dashed lines, respectively.

Moreover, $T$ Si-Ge interface modes, sharply localized at the interfaces between the Si and Ge layers, are found to fall around 400 cm$^{-1}$, in the gap between the TO bulk branches of Si and Ge.[16]

As in GaAs/AlAs SL's, confined SL frequencies can be related to the corresponding bulk dispersions.[4] Within a simple "standing-wave" model, an effective confinement wave vector $q_m$ can be associated with the $m$th confined mode:

$$q_m = 2m2\pi/[a_0(n+\gamma)] , \tag{1}$$

where $n$ is the nominal number of atomic planes in the vibrating (Si or Ge) region, $a_0$ is the bulk lattice parameter, and $\gamma$ accounts for penetration of the envelope function of the displacements into adjacent layers.[17] With the correct choice of $\gamma$, the frequency $\omega_m$ of the $m$th confined mode will be such that

$$\omega_m = \omega^{\text{bulk}}(q_m) , \tag{2}$$

provided that $\omega^{\text{bulk}}(q)$ is the bulk Si or Ge dispersion in the appropriate strain configuration.[7] For a strain-symmetrized $Si_n/Ge_n$ SL, we will have to refer to the bulk dispersions corresponding to lattice matching to $Si_{0.5}Ge_{0.5}$ (dashed lines in Fig. 1).

Figure 3 shows the frequencies of the Si-like $m=1$ and 3 modes for the $L$ and two $T$ polarizations ($T1$ and $T2$)

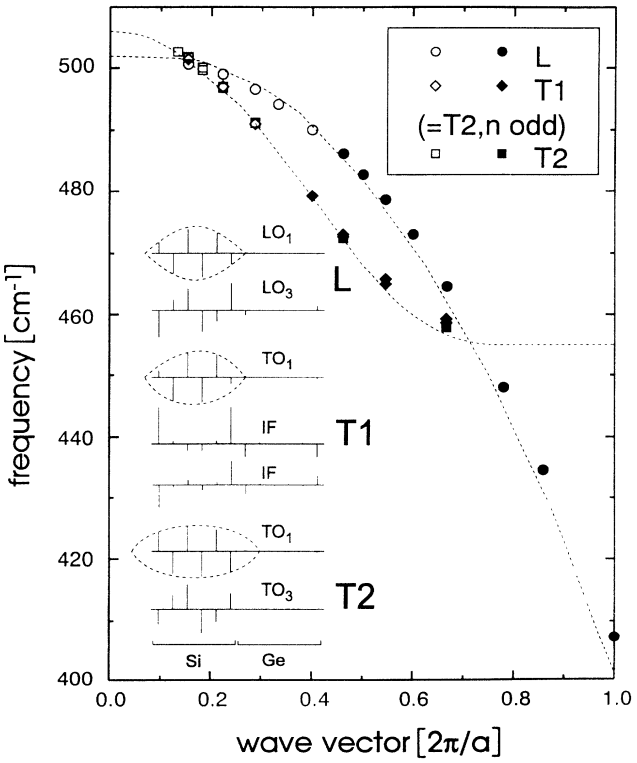


FIG. 3. Calculated frequencies of $L$ and $T$ Si-like modes of strain-symmetrized $Si_n/Ge_n$ *ideal* SL's, unfolded onto the corresponding bulk dispersion according to Eq. (1). Values of $\gamma$ are $\gamma=1$ for $L$ ($n$ even or odd) and $T1$ modes ($n$ even), $\gamma=2$ for $T1$ and $T2$ modes ($n$ odd), and $\gamma=3$ for $T2$ modes ($n$ even). Empty and full symbols denote $m=1$ and 3 modes, respectively. The inset shows the displacement amplitude of a $Si_6/Ge_6$ SL.

for strain-symmetrized $Si_n/Ge_n$ SL's with ideally sharp interfaces and $n=4$-12. They are plotted as a function of $q_m$ in the first half of the Brillouin zone (BZ), together with the corresponding strained bulk branches. The parameter $\gamma$ in Eq. (1) was taken as follows: $\gamma=1$ for the $L$ ($n$ even or odd) and $T1$ ($n$ even) polarizations, $\gamma=2$ for $T1$ and $T2$ ($n$ odd; in this case $T1$ and $T2$ are degenerate due to the tetragonal symmetry), and $\gamma=3$ for the $T2$ polarization ($n$ even). The mapping ("unfolding") onto the bulk dispersion is very good with this choice.

The different values of $\gamma$ are due to the dependence of the phonon spectrum and mode confinement on the mode symmetry, as shown by the displacement patterns for $n=6$ in the inset of Fig. 3. For the $L$ polarization the displacement pattern is similar for any choice of $n$, with $\gamma=1$. For $T$ vibrations we have to consider that the interplanar forces connecting atomic planes are of two different types, one much stronger than the other, and alternate along the [001] direction.[9] If $n$ is even for a given $T$ polarization ($T1$), both interfaces are strongly coupled, while for $T2$ the interface bonds are light. This is the reason why two interface modes arise for $T1$ while there are no interface modes for $T2$. Interface planes involved in interface modes do not participate in Si-like vibrations, since the modes must orthogonalize to each other. This leads us to the values $\gamma=1$ for $T1$ and $\gamma=3$ for $T2$, which are consistent with the displacement patterns. For $n$ odd, one of the two interfaces in the SL unit cell has a strong bond, while the other one is weak, giving rise to a single interface mode. As a result, in this case $\gamma=2$. Thus for ideal structures the frequencies of Si-like confined optical modes can be described by the simple unfolding rule (1) and appropriate values of $\gamma$.

The left-hand panel of Fig. 2 shows the in-plane dispersion for the same (001)-oriented $Si_8/Ge_8$ SL versus in-plane wave vector along [100]. As reported previously,[10] we find that optical modes become dispersive for propagation away from the growth direction. However, close to the zone center their in-plane dispersion is in general weak compared to acoustic modes. As expected for nonpolar SL's, the optical-phonon spectra are isotropic close to the zone center, contrary to the well-known behavior of GaAs/AlAs structures.[6]

### B. Experimental results

Figure 4 shows experimental Raman spectra of a (001)-$Si_8/Ge_8$ SL in different scattering configurations. The upper spectrum was taken from the as-grown surface in the $z(x',x')$-$z$ configuration, while the lower ones were observed from various surfaces with different polarizations of incident and scattered light.

In order to interpret these spectra, we first introduce a brief discussion of the relevant selection rules. In backscattering from the (001) surface, for the odd confined-optical-phonon modes these can be derived—to a first-order approximation—from the $O_h$ point-group Raman tensors of the bulk materials, thus neglecting any consequences of phonon confinement on the selection rules. The result is compiled in the topmost part of Table I. The even-order modes are expected to have negligible intensity due to their symmetry, which results in a vanishing dipole moment.

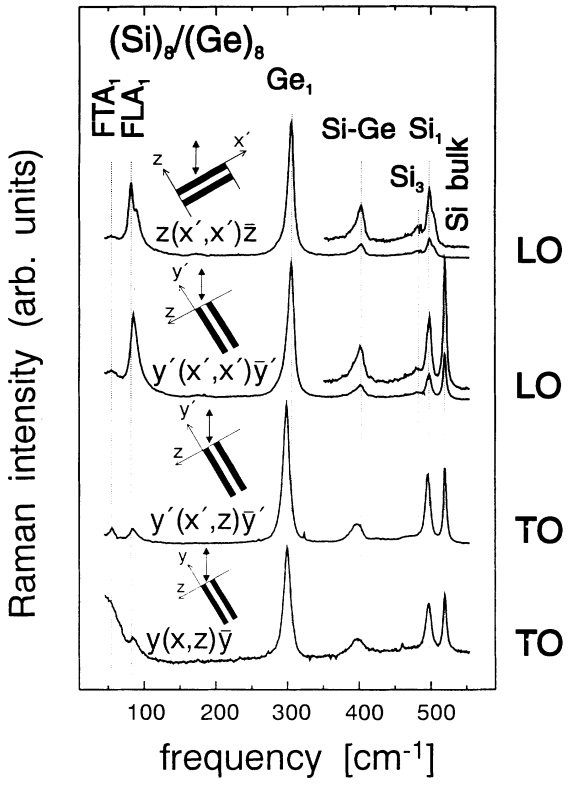


FIG. 4. Micro-Raman spectra of a (001)-$Si_8/Ge_8$ SL taken from the (001), (110), and (010) surfaces with laser wavelength $\lambda=514.5$ nm. The scattering configurations are shown as insets.

We also use the bulk point group $O_h$ for establishing the selection rules for in-plane scattering. Note, however, that in Table I the labeling of the polarizations (TO and LO) is taken with respect to the growth direction rather than the direction of the transferred photon momentum. (In practice, this means that in-plane phonon modes are labeled TO- and LO-like simply according to their frequency range.) This is due to the fact that we have to take into account the momentum associated with optical-phonon quantization, which is considerably larger than that of the photons. Because the confinement wave vector is only an effective wave vector and is not associated with phonon propagation, this notation is only conventional (at the $\Gamma$ point we have longitudinal modes labeled TO, and vice versa[20]). As concerns optical modes, the important point to be retained from Table I is that—despite their negligible dispersion—micro-Raman still yields additional information with respect to the usual backscattering from the growth surface alone, since for geometric reasons it gives access to additional polarizations.

Given these selection rules, we now come to the interpretation of the spectra of Fig. 4. From Table I we find that only longitudinal modes are expected in the upper spectrum [backscattering from the as-grown surface in the $z(x',x')$-$z$ configuration]. The $m=1$ Ge-like and the

$m=1$ the 3 Si-like $L$ modes are resolved. As expected, they are shifted with respect to the bulk LO($\Gamma$) frequency due to confinement, and to the built-in strain in the Si and Ge layers.[7,18,19] The peak around 400 $cm^{-1}$, which is not expected for ideal SL's in the $L$ polarization, is attributed to a Si-Ge alloylike vibration, due mainly to interface roughness.[9]

The spectra in the lower part of Fig. 4 correspond to in-plane wave vectors. They all show an additional peak from the Si substrate, since in this case the SL thickness is smaller than the laser spot diameter. Comparing the $z(x',x')$-$z$ spectrum from the as-grown surface to the $y'(x',x')$-$y'$ spectrum from the (110) edge, we find the optical phonons to be similar. This confirms that the dependence on the scattering wave vector $q$ is negligible for the optical modes. In contrast, the optical-phonon modes in the $y'(x',z)$-$y'$ and $y(x,z)$-$y$ spectra taken along [110] and [010] are shifted in energy and are of different relative intensities. With reference to Table I, these modes are attributed to TO modes. Since they are expected to be polarized along different directions, the similarity of the last two spectra indicates that the confined-TO modes are degenerate, which is expected for tetragonal symmetry.

Measuring various in-plane configurations for this sample, we found good agreement with the modified bulk selection rules, although some relaxation—attributed to surface roughness caused by sample preparation and to scattering from the growth surface—is observed. Strain relaxation due to polishing was investigated by comparing the $z(x',x')$-$z$ and $y'(x',x')$-$y'$ spectra. As expected, partial strain relaxation detected from a shift of the optical phonons was observed for asymmetrically strained SL's, whereas the strain-symmetrized SL's remain stable.

We have performed a similar study for a series of $Si_n/Ge_n$ SL's ($n=4$, 5, 6, 8, and 12) grown on strain-symmetrizing alloy buffers. From measurements in backscattering configuration along the [110] direction, $L$ and $T$ modes are easily distinguished by the polarization of the light. The results are plotted as full symbols in Figs. 5 and 6, respectively, together with the calculated frequencies of Fig. 2, following the unfolding rule (1). For simplicity, we use $\gamma=1$ for $L$ and $\gamma=2$ for $T$ polarization. It appears very clearly that—contrary to the

TABLE I. Raman- and Brillouin-scattering selection rules for backscattering from (001) and (110) surfaces, derived from the $O_h$ point group for different scattering geometries. For Brillouin scattering, $q\|[001]$ is assumed. In the case of the SL the photoelastic constants $p_{ij}$ are the Fourier components of $|p_{ij}(\mathrm{Si})-p_{ij}(\mathrm{Ge})|$. The phonon polarization is labeled with respect to the wave vector of the SL periodicity (see text). $x$:[100], $y$:[010], $z$:[001], $x'$:[1$\bar{1}$0], $y'$:[110], $z'=z$:[001].

| | | | | Bulk | | |
|---|---|---|---|---|---|---|
| | Raman scattering | | | Brillouin scattering | | |
| [001] | $x$(TO) | $y$(TO) | $z$(LO) | $x$(TA) | $y$(TA) | $z$(LA) |
| $z(x,x)\bar{z}$ | 0 | 0 | 0 | 0 | 0 | $p_{12}^2$ |
| $z(x,y)\bar{z}$ | 0 | 0 | $d^2$ | 0 | 0 | 0 |
| $z(x',x')\bar{z}$ | 0 | 0 | $d^2$ | 0 | 0 | $p_{12}^2$ |
| $z(x',y')\bar{z}$ | 0 | 0 | 0 | 0 | 0 | 0 |
| [110] | $x'$(TO) | $z$(TO) | $y'$(LO) | $x'$(TA) | $z$(TA) | $y'$(LA) |
| $y'(x',x')\bar{y}$ | 0 | $d^2$ | 0 | 0 | 0 | $[(p_{11}+p_{12})/2-p_{44}]^2$ |
| $y'(x',z)\bar{y}$ | $d^2$ | 0 | 0 | 0 | 0 | 0 |
| $y'(z,z)\bar{y}$ | 0 | 0 | 0 | 0 | 0 | $p_{12}^2$ |
| | | | | Superlattice | | |
| | Raman scattering | | | Brillouin scattering ($q\|[001]$) | | |
| [001] | $x$(TO) | $y$(TO) | $z$(LO) | $x$(TA) | $y$(TA) | $z$(LA) |
| $z(x,x)\bar{z}$ | 0 | 0 | 0 | 0 | 0 | $p_{12}^2$ |
| $z(x,y)\bar{z}$ | 0 | 0 | $d^2$ | 0 | 0 | 0 |
| $z(x',x')\bar{z}$ | 0 | 0 | $d^2$ | 0 | 0 | $p_{12}^2$ |
| $z(x',y')\bar{z}$ | 0 | 0 | 0 | 0 | 0 | 0 |
| [010] | $x$(TO) | $y$(TO) | $z$(LO) | $x$(TA) | $y$(TA) | $z$(LA) |
| $y(x,x)\bar{y}$ | 0 | 0 | 0 | 0 | 0 | $p_{12}^2$ |
| $y(x,z)\bar{y}$ | 0 | $d^2$ | 0 | $p_{44}^2$ | 0 | 0 |
| $y(x+z,x+z)\bar{y}$ | 0 | $d^2$ | 0 | $p_{44}^2$ | 0 | $(p_{11}+p_{12})^2/4$ |
| $y(x+z,x-z)\bar{y}$ | 0 | 0 | 0 | 0 | 0 | $(p_{12}-p_{11})^2/4$ |
| $y(z,z)\bar{y}$ | 0 | 0 | 0 | 0 | 0 | $p_{11}^2$ |
| [110] | $x'$(TO) | $y'$(TO) | $z$(LO) | $x'$(TA) | $y'$(TA) | $z$(LA) |
| $y'(x',x')\bar{y}'$ | 0 | 0 | $d^2$ | 0 | 0 | $p_{12}^2$ |
| $y'(x',z)\bar{y}'$ | $d^2$ | 0 | 0 | $p_{44}^2$ | 0 | 0 |
| $y'(z,z)\bar{y}'$ | 0 | 0 | 0 | 0 | 0 | $p_{11}^2$ |

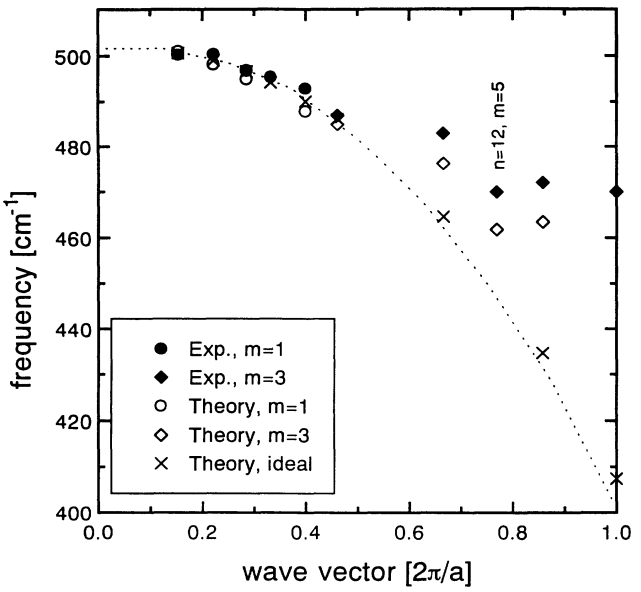


FIG. 5. Experimental (full symbols) and calculated (empty symbols) frequencies of $L$ Si-like modes of strain-symmetrized $Si_n/Ge_n$ SL's, unfolded onto the corresponding bulk dispersion according to Eq. (1) with $\gamma=1$. Circles and diamonds correspond to $m=1$ and 3 modes, respectively. The calculations are for intermixed SL's with three monolayers of $Si_xGe_{1-x}$ at interfaces ($x=0.25$, 0.50, and 0.75). As a reference, the frequencies calculated for ideal SL's from Fig. 3 are also given (crosses). The dotted line is the corresponding strained bulk dispersion.

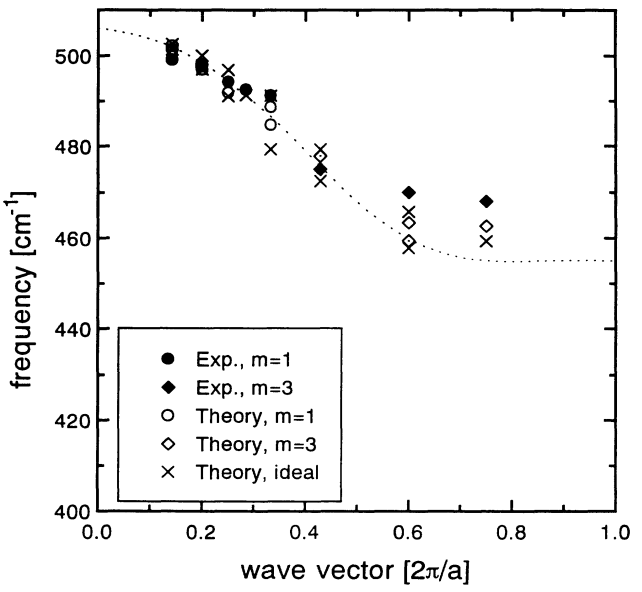


FIG. 6. Experimental and calculated frequencies of $T$ Si-like modes of strain-symmetrized $Si_n/Ge_n$ SL's, unfolded onto the corresponding bulk dispersion according to Eq. (1) with $\gamma=2$. The calculations are for intermixed SL's with three monolayers of $Si_xGe_{1-x}$ at interfaces with $x=0.25$, 0.50, and 0.75, respectively, and for the ideal SL's. Notations are as in Fig. 5.

theoretical findings for ideal SL's (Fig. 3)—both $L$- and $T$-polarized modes deviate considerably from the strained bulk dispersions (dotted lines in Figs. 5 and 6). The deviation is most pronounced for $L$ modes associated with large $q_{\text{eff}}$. For $T$ modes, however, the main discrepancy is the absence of a splitting in the experiment. These effects will be discussed in Sec. IV C.

In Fig. 7 the linewidths of the optical phonons are plotted for $Si_n/Ge_n$ SL's for the $y'(x',x')$-$y'$ ($L$) and $y'(x',z)$-$y'$ ($T$) polarizations. For the Si-like mode, the $T$ peaks are in general broader, especially for the $Si_3$ mode. This might be due to a small residual splitting between $T1$ and $T2$ polarizations even for intermixed SL's, as will be shown in Sec. IV C. The linewidth of the SiGe-like mode around 400 cm$^{-1}$ is considerably smaller in the $L$ as compared to the $T$ polarization. The nature of this mode is extensively discussed in Ref. 9 on the basis of that discussion, the sharper $L$ line shape is attributed to its stronger spatial localization. For the Ge-like modes the $T$ line shape is always narrower than the $L$ for the thinnest Ge layers, whereas the behavior is opposite for the thicker Ge layers. $T$ Ge-like modes are expected to be confined more rigorously within the Ge layers since there is no overlap of the [001]-TO Ge and TA Si bulk dispersion branches. The corresponding $L$ branches overlap and thus the confined $L$ Ge-like modes have a resonant propagative nature.[15] This means that the ex-

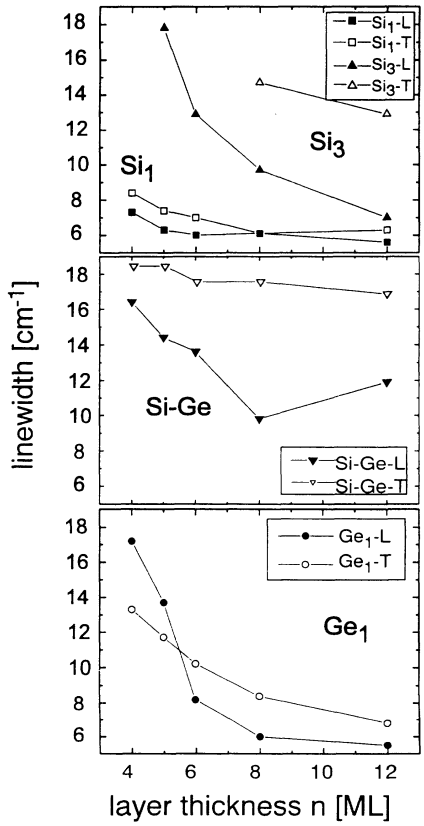


FIG. 7. Linewidths of optical modes of $Si_n/Ge_n$ SL's, as obtained from spectra taken from the (110) surface. Full and empty symbols denote $L$- and $T$-like modes, respectively.

tension of the confined $T$ Ge-like modes to the disordered interface region is smaller, and therefore the disorder induced inhomogeneous broadening must be smaller as compared to $L$ modes. The effect is expected to be more pronounced for very thin layers, for which the relative interface contributions is larger. Therefore the narrowing of the confined $T$ Ge-like modes as compared to the $L$ modes is evidence of their less dispersive nature. For the thicker layers, however, the inhomogeneous broadening should be small even in the $L$ polarization. The broadening of the $T$ mode in this case might again be due to a small residual splitting between $T1$ and $T2$.

### C. Theoretical results for intermixed superlattices

To explain the origin of the discrepancy between experimental results and theoretical predictions for ideal SL's, we have performed calculations which take into account interface roughness by assuming three intermixed $Si_xGe_{1-x}$ alloylike layers at the interfaces, with symmetric or asymmetric (e.g., $x=0.25$, 0.50, and 0.75) profiles. The results are shown by open symbols in Figs. 5 and 6. As for experimental data, all values are plotted for $\gamma=1$ and 2 for $L$ and $T$ modes, respectively (the unfolding rules derived for the ideal structures have no meaning for the intermixed SL's). Now the agreement between theoretical and experimental results both for $L$ and $T$ polarizations is much closer, with the calculated frequencies also falling also considerably above the bulk dispersion for large $q_{\text{eff}}$.

Note that for the $T$ polarization, a splitting between $T1$ and $T2$ remains for $n$ even in our theoretical results, although much smaller than expected for ideal SL's. Thus $n_{\text{eff}}$ still depends slightly on the SL symmetry. We believe the splitting between different scattering configurations very difficult to observe experimentally, since every monoatomic step on the substrate would rotate the SL unit cell by 90°, thus interchanging the role of $T1$ and $T2$ symmetries. Therefore the expected experimental line shape should be a superposition of the two for $T$-allowed configurations. This is consistent with the broader line shape observed experimentally for $T$ modes as compared with $L$ modes (Fig. 7).

These results can be interpreted as follows. The modes whose frequency falls above the alloy bands of the interface alloy layers are confined in the pure Si layer. This is the case for modes with small $q_{\text{eff}}$, which therefore map quite closely to the bulk dispersion for $\gamma=1$. Modes assigned to large values of $q_{\text{eff}}$ fall within the alloy bands. Thus they extend further into the alloy layers, which explains their large deviation from the bulk dispersion. An effective confinement length $d_{\text{eff}}$ can be extracted from the calculated local density of states for a given intermixing configuration.[9] This leads to $\gamma\cong 0$ for $LO_1$ modes, while for higher-order modes $\gamma=2$–2.5. Using these values, the LS mode frequencies map closely onto the bulk dispersion.

We have therefore shown that simple models of interface mixing account for the experimentally observed deviation between unfolded Si-like SL mode frequencies and the bulk dispersion.[21]

## V. ACOUSTIC MODES

As is apparent from Fig. 2, a prominent feature of the SL spectra is the existence of equidistant folded-acoustic doublets due to the artificial periodicity in the growth direction. As long as these modes originate from the linear part of the bulk dispersions, their Γ-point frequencies are very well described by the elastic continuum model of Rytov.[22,4] Their in-plane dispersion is found to be larger than for optical modes, as apparent from the left-hand panel of Fig. 2.

In Fig. 8 we compare the $z(x',x')$-$z$ and the in-plane $y'(x',x')$-$y'$ spectra of the $Si_8/Ge_8$ SL. Thus we can study the effect of an in-plane momentum transfer on the frequencies of the folded-acoustic modes. A shift of 3 $cm^{-1}$ in the energy of the first folded LA ($FLA_1$) peak is observed, and the doublet structure of the peak is lost. In the inset of Fig. 8 general features of the acoustic in-plane dispersion are represented schematically. The effect on the $m=-1$ branch is more pronounced as compared to the $m=+1$ branch. Since $q$ has a finite value due to the backscattering geometry, the energy of the $m=-1$ peak is expected to increase for in-plane $q$, because the dispersion of this branch is upwards instead of downwards, as for $q$ parallel to the growth direction. The $m=+1$ branch is upwards in both cases, and so the $m=+1$ peak

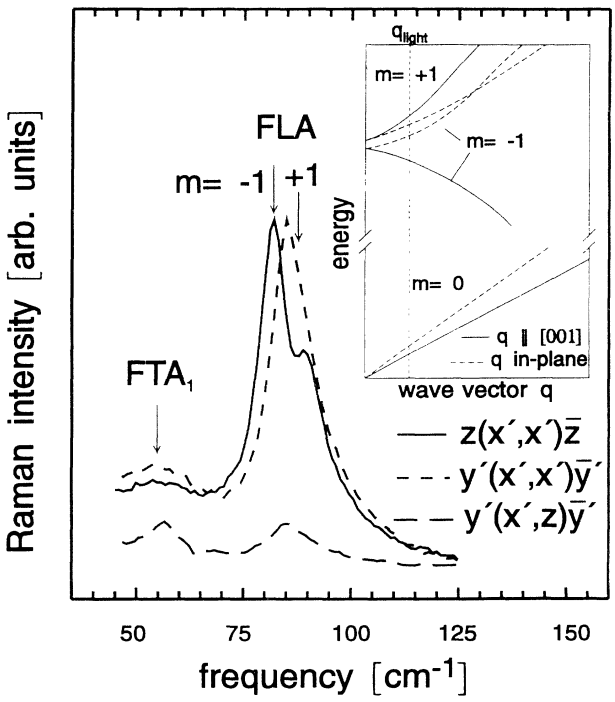


FIG. 8. Folded-acoustic modes of the $Si_8/Ge_8$ SL for scattering from the (001)-growth plane and from the (110) edge. Schematic features of the $FLA_1$ region of the dispersion near the Γ point are shown in the inset for wave vectors parallel (solid lines) and perpendicular (dashed lines) to the growth direction. The vertical dashed line indicates momentum transfer by the light.

should remain rather constant. The doublet structure disappears, since the two peaks are now too close together to be resolved.

In order to understand the intensity of the peaks, we need also to discuss the selection rules for the case of acoustic modes. As concerns scattering from the growth surface, for a rough determination of the selection rules of the folded-acoustic modes—neglecting, for instance, the doublet splitting—the Brillouin tensors of the bulk materials (Table I) can be used, as the elastooptic mechanism dominates the scattering of these modes.[23] The lower point symmetry of the SL is thus neglected. For scattering parallel to the growth direction, a detailed analytical analysis on the absolute scattering intensity of folded-acoustic modes in (001)-GaAs/AlAs SL's was given by He, Djafari-Rouhani, and Sapriel.[23] A numerical approach, also including SL's with layer intermixing, was used by Jusserand *et al.*[24]

For scattering perpendicular to the growth direction, to our knowledge no detailed theory has been worked out so far. For Brillouin scattering a mode is active due to the finite $q$ induced by the momentum transfer of the light, whereas the Raman selection rules are valid for $q$ exactly equal to zero. Consequently we have to consider the effective wave vector $q^*_{\text{eff}}$—which in the case of the folded-acoustic modes corresponds to the actual wave vector in the extended-zone scheme (i.e., depending only on the SL period)—not only for the determination of the transverse or longitudinal character of the phonons, as done for the confined-optical modes, but also for the scattering mechanism. Since for short-period SL's $q^*_{\text{eff}}$ is much larger than the photon momentum, for in-plane scattering we will also use the Brillouin tensors appropriate for $q$ parallel to the growth direction.

In the bulk case $q$ is parallel to the scattering wave vector. Both cases are identical for backscattering from the growth plane. The labeling TA and LA in Table I refers to the direction of $q^*_{\text{eff}}$, i.e., the growth direction. In close analogy to confined-optical modes, these modes are TA- and LA-like. Thus in the $y'(x',x')$-$y'$ configuration we expect a FLA mode with the same intensity as in $z(x',x')$-$z$, which is consistent with the spectra in Fig. 8. The $y(z,z)$-$y$ spectrum showed no significant $\text{FLA}_1$ intensity, though the selection rules yield $(p_{11})$.[2] In the $y'(x',z)$-$y'$ geometry, a pronounced peak appears with an energy which is expected for the $\text{FTA}_1$ mode, whereas the $\text{FLA}_1$ mode is much weaker than in the polarized spectra. The presence of FTA modes in depolarized spectra is in agreement with Table I. However, a much broader structure around the first folded TA (FTA) frequency is also observed in the polarized spectra, although TA modes are forbidden for parallel polarization by the bulk selection rules. The mechanism which allows their observation in this case is not yet clearly understood.[25] In general, we found that within the experimental error the observed intensities of the folded-acoustic modes are consistent with the selection rules of Brillouin scattering with $q$ parallel to the growth direction, if we assume $p_{11}$, $p_{44} \ll p_{12}$. A more detailed theory based on the photoelastic mechanism is needed for in-plane backscattering, but our model may serve as a rough approximation.

## VI. DISCUSSION AND SUMMARY

By performing in-plane Raman scattering on Si/Ge SL's grown along (001), we were able to observe optical and acoustical modes, both with $L$ and $T$ polarizations. The polarization character of the confined-optical and folded-acoustic modes was found to be governed by the wave vector corresponding to the confinement length or SL periodicity, respectively. A Brillouin mechanism determines the intensities of the folded-acoustic modes; however, contrary to the bulk case, the relevant $q$ is no longer given by the scattering wave vector but by the SL periodicity. For in-plane scattering the frequencies of the FLA modes increase due to the photon momentum transfer and the in-plane dispersion; such dispersion was found to be negligible for confined modes.

We have interpreted our experimental data in terms of first-principles calculations of the phonon spectra. For ideal SL's, theoretical results delivered simple unfolding rules for mapping confined LO and TO modes onto the bulk dispersion. The deviations from such rules observed in the experimental data were shown to be due to interface roughness. As found in previous studies of GaAs/AlAs structures,[12] a simple model assuming the existence of a thin intermixed alloy layer at the interfaces is therefore able to account for the Raman spectra of thin superlattices.

## ACKNOWLEDGMENTS

We would like to thank B. Jusserand and M. Haines for fruitful discussions. The experimental work was supported by ESPRIT Basic Research Project No. 7128, the calculations were supported by CNR under Grant No. 92.01598.FP69.

[1]G. Abstreiter, K. Eberl, E. Friess, W. Wegscheider, and R. Zachai, J. Cryst. Growth **95**, 431 (1989).

[2]See, e.g., *Silicon Molecular Beam Epitaxy*, edited by J. C. Bean, S. S. Iyer, and K. L. Wang, MRS Symposium Proceedings No. 220 (Materials Research Society, Pittsburgh, 1991).

[3]U. Menczigar, G. Abstreiter, J. Olajos, H. Grimmeis, H. Kibbel, and H. Presting, Phys. Rev. B **47**, 4099 (1993).

[4]See, e.g., the reviews: B. Jusserand and M. Cardona, in *Light Scattering in Solids V*, edited by M. Cardona and G. Guntherodt (Springer, Berlin, 1989), p. 49; J. Menéndez, J. Lumin. **44**, 285 (1989).

[5]R. Hessmer, A. Huber, T. Egeler, M. Haines, G. Tränkle, G. Weimann, and G. Abstreiter, Phys. Rev. B **46**, 4071 (1992).

[6]G. Scamarcio, M. Haines, G. Abstreiter, E. Molinari, S. Baroni, A. Fischer, and K. Ploog, Phys. Rev. B **47**, 1483 (1993).

[7]A. Qteish and E. Molinari, Phys. Rev. B **42**, 7090 (1990); A. Fasolino, E. Molinari, and A. Qteish, in *Condensed Systems of*

*Low Dimensionality,* edited by J. L. Beeby *et al.* (Plenum, New York, 1991), p. 495.

[8]S. de Gironcoli, Phys. Rev. B **46**, 2412 (1992).

[9]S. de Gironcoli, E. Molinari, R. Schorer, and G. Abstreiter, Phys. Rev. B **48**, 8959 (1993).

[10]Three-dimensional calculations were available from phenomenological models; see, e.g., A Ghanbari, J. D. White, G. Fasol, C. J. Gibbings, and C. G. Tuppen, Phys. Rev. B **42**, 7033 (1990).

[11]K. Eberl, E. Friess, W. Wegscheider, U. Menczigar, and G. Abstreiter, Thin Solid Films **183**, 95 (1989); E. Kasper, in *Physics and Application of Quantum Wells and Superlattices,* edited by E. E. Mendez and K. von Klitzing, Vol. 170 of *Advanced Study Institute NATO Series B: Physics* (Plenum, New York, 1987), p. 10.

[12]E. Molinari, S. Baroni, P. Giannozzi, and S. de Gironcoli, Phys. Rev. B **45**, 4280 (1992).

[13]G. Dolling, *Inelastic Scattering of Neutrons in Solids and Liquids* (IAEA, Vienna, 1963), Vol. II, p. 37; G. Nilsson and G. Nelin, Phys. Rev. B **6**, 3777 (1972); **3**, 364 (1971).

[14]S. de Gironcoli and S. Baroni, Phys. Rev. Lett. **69**, 1959 (1992).

[15]A. Fasolino, E. Molinari, and J. C. Maan, Phys. Rev. B **39**, 3923 (1989).

[16]A. Fasolino and E. Molinari, J. Phys. (Paris) Colloq. **5**, C5-69 (1987); E. Molinari and A. Fasolino, Appl. Phys. Lett. **54**, 1220 (1990).

[17]E. Friess, K. Eberl, U. Menczigar, and G. Abstreiter, Solid State Commun. **73**, 203 (1990).

[18]Jian Zi, Kaiming Zang, and Xide Xie, Phys. Rev. B **45**, 9447 (1992).

[19]E. Anastassakis, in *Light Scattering in Semiconductor Structures and Superlattices,* edited by D. J. Lockwood and J. F. Young, Vol. 273 of *Advanced Study Institute NATO Series B: Physics* (Plenum, New York, 1991), p. 173.

[20]J. E. Zucker, A. Pinczuk, D. S. Chemla, A. Gossard, and W. Wiegmann, Phys. Rev. Lett. **53**, 1280 (1984).

[21]In the present study, the assumed model for interface roughness is limited to intermixed layers with *short-range* compositional disorder. Possible distinct effects of long-range terrace-like roughness on optical modes are discussed elsewhere: S. de Gironcoli and E. Molinari, in *Proceedings of the Sixth International Conference on Modulated Semiconductor Structures (MSS-6), Garmisch, Germany, 1993* [Solid-State Electron (to be published)].

[22]S. M. Rytov, Sov. Phys. Acoust. **2**, 68 (1956).

[23]J. He, B. Djafari-Rouhani, and J. Sapriel, Phys. Rev. B **37**, 4086 (1988).

[24]B. Jusserand, D. Paquet, F. Mollot, F. Alexandre, and G. LeRoux, Phys. Rev. B **35**, 2808 (1987).

[25]M. I. Alonso, F. Cerdeira, D. Niles, M. Cardona, and H. Kibbel, J. Appl. Phys. **66**, 5645 (1990).

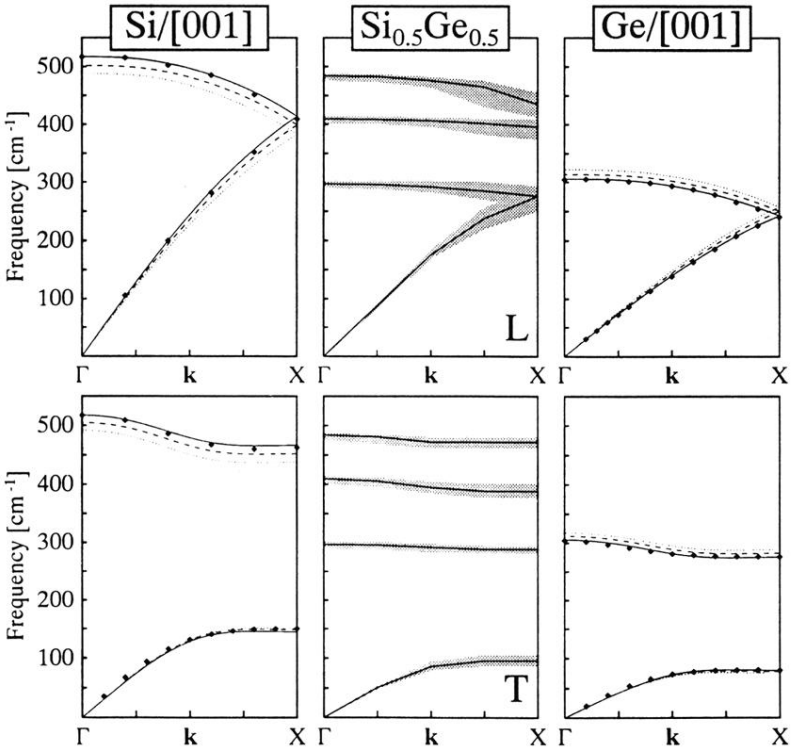


FIG. 1. Calculated bulk dispersions along (001) for Si and Ge and the $Si_{0.5}Ge_{0.5}$ alloy. *L* and *T* polarizations are shown in the top and bottom panels, respectively. For Si and Ge, different strain configurations are shown: unstrained (solid lines), and lattice matched to the $Si_{0.5}Ge_{0.5}$ alloy (dashed lines) or to the other semiconductor (dotted lines). The symbols are neutron-scattering data for the unstrained configuration. The shaded lines in the central panel indicate the width of the alloy quasidispersion (see Ref. 9).